Scanning Microscopy Vol. 11, 1997 (Pages 367-374) 0891-7035/97$5.00+.25
Scanning Microscopy International, Chicago (AMF O'Hare), IL 60666 USA

SIMULATIONS OF ELECTRON HOLOGRAMS OF LONG RANGE ELECTROSTATIC FIELD

Giorgio Matteucci*, Gianfranco Missiroli and Giulio Pozzi

Department of Physics and Istituto Nazionale per la Fisica della Materia, University of Bologna, Bologna, Italy

Abstract

The basic principles of off-axis image electron holography applied to the investigation of long range electrostatic fields are presented. The effects of the perturbed reference wave and of the boundary conditions on the reconstructed holograms are illustrated by means of computer simulations referring to the cases of charged dielectric spheres and microtips.

Key Words: Electron holography, electrostatic field mapping, charged dielectric spheres, biased microtips.

*Address for correspondence:
Department of Physics and Istituto Nazionale per la Fisica della Materia, University of Bologna
viale B. Pichat 6/2, 40127 Bologna, Italy
Telephone number: +39-051-2095145
FAX number:+39-051-2095153
E-mail:mateucci@df.unibo.it

Introduction

The interest of our group in electron holography was motivated by its peculiar capability to display useful information in the investigation of magnetic (Matteucci *et al*., 1984) and electric fields. During the study of reverse-biased p-n junctions (Frabboni *et al*., 1987), the problems encountered in the reconstruction of the holograms demonstrated unambiguously that the long range field perturbed the so-called reference wave. A basic assumption of holography was thus manifestly violated and in order to assess the consequences of this fact we started to investigate other specimens with long range electric fields, like charged dielectric particles (Chen *et al*., 1989; Matteucci *et al*., 1991) or biased tips (Matteucci *et al*., 1992), having with respect to p-n junctions the advantages of an easier specimen preparation and of a simpler theoretical description. The main experimental results have been reviewed in a recent paper (Matteucci *et al*., 1996).

The aim of this work is to mainly emphasize the theoretical aspects, since the above mentioned investigations have evidenced that a good modelling is essential in order to interpret some puzzling features of the reconstructed holographic images, which at first sight seem to contradict the naive expectations and whose explanation allows us to extract the maximum information from the obtained experimental results. Therefore, the basic principles of the method and the related equations are briefly recalled and models for the electric field and the associated phase shift arising from charged dielectric spheres and biased tips will be presented.

It will be shown that by using the powerful software package Mathematica (Wolfram, 1994), most of the calculations can be carried out by the program often in an analytical way. Moreover the software allows an easier and quicker presentation of the results of the simulations in an outstanding graphical form with respect to standard Fortran, thus allowing the attention to be focussed on the physical problems involved rather than on the programming.

Basic Theoretical Considerations

By considering only elastic scattering events, the

interaction of the specimen with the electron beam can be described through a complex transmission function (object wave-function) $\Psi(\mathbf{r})$ which represents the ratio between the complex amplitudes of the out-going and the in-going electron wave-functions; $(\mathbf{r}) = (x,y)$ is a bidimensional vector perpendicular to the optic axis z which is parallel and in the same direction as the electron beam. In the standard phase-object approximation:

$$\psi(\mathbf{r}) = C(\mathbf{r}) \exp[i\phi(\mathbf{r})] \tag{1}$$

where $C(\mathbf{r})$ is the object amplitude and the phase term $\phi(\mathbf{r})$ is given by:

$$\phi(\mathbf{r}) = (\pi/\lambda E) \int_l V(\mathbf{r},z)dz \tag{2}$$

The integral is taken along a trajectory l parallel to the optical axis z inside and outside the specimen to include stray fields, $V(\mathbf{r},z)$ is the electrostatic potential, E is a parameter linked to the accelerating voltage and equal to it in the non-relativistic approximation, and λ is the electron wavelength.

As the recorded signal in conventional imaging is proportional to the square modulus of the image wave-function, neglecting aberrations, it turns out that:

$$I(\mathbf{r}) = |\Psi(\mathbf{r})|^2 = |C(\mathbf{r})|^2 \tag{3}$$

showing that the phase information is completely lost in the Gaussian image of the object.

Contrary to standard phase-contrast techniques (Chapman, 1984), which only allow a partial recovering of this information, electron holography is the unique method by means of which it is possible to obtain the complete retrieval of the two-dimensional image wave-function and to display and evaluate its phase in a vivid and, more important, a quantitative way. This is accomplished in the off-axis image scheme by superimposing, within the electron microscope, a tilted coherent plane reference wave $R = \exp[2\pi i x u_c]$ with carrier spatial frequency u_c on an image of the object wave-function.

Both wave front and amplitude beam splitting devices can be used for realizing this task (Missiroli *et al*., 1981). However, the most widely used and versatile type of electron interferometer is the Möllenstedt and Düker (1956) electron biprism which belongs to the class of wavefront division interferometers.

Let us analyze first the ideal situation, reported in Figure 1a, in which a plane wave (PW) illuminates a specimen S. Only that part of the wave which has passed through S suffers a phase modulation. The reference wave R travels outside the specimen through a field free region and is not affected by any field (Matteucci *et al*., 1991). The biased biprism provides the splitting of the incoming wave front

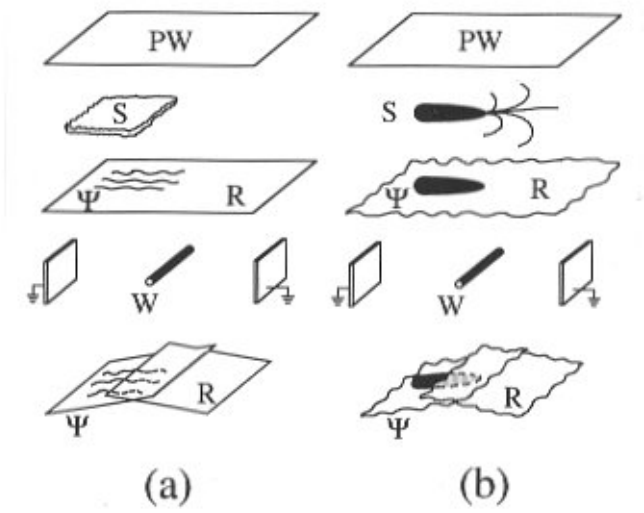

Figure 1. Sketch of electron hologram formation with: (**a**) a reference plane wave and (**b**) a perturbed reference wave. PW: incident plane wave; S: specimen; Ψ and R: object and reference wave; and W: biprism wire.

and the subsequent superposition of the object wave Ψ and the reference wave R.

In these conditions the intensity recorded in the interferogram, henceforth called hologram, is given by:

$$\begin{aligned} H &= |R+\Psi|^2 = |R|^2 + |\Psi|^2 + \Psi^* R + \Psi R^* \\ &= 1 + C(\mathbf{r})^2 + 2C(\mathbf{r})\cos[2\pi u_c x + \phi(\mathbf{r})] \end{aligned} \tag{4}$$

showing that both amplitude C and phase ϕ of the image wave-function are encoded in the hologram, contrary to a conventional recording whose intensity is given by Equation (3).

The situation is completely different when the specimen gives rise to long range electric and/or magnetic fields as sketched in Figure 1b. A charged tip is shown which generates a field extending all around it perturbing the electron wave front.

The resulting reference wave is no longer given by $R = \exp[2\pi i x u_c]$ but is multiplied by the phase factor $\exp[i\phi(\mathbf{r}+\mathbf{D})]$, where $\mathbf{D} = (D,0)$ is the vector that connects the points brought to interfere, D being defined as "interference distance". Therefore, in this case, as can be shown by a simple analysis (Matteucci *et al*., 1991), the hologram stores the information due to a fictitious specimen whose amplitude and phase are given by:

$$C(\mathbf{r}) \text{ and } \Delta\phi(\mathbf{r}) = \phi(\mathbf{r}) - \phi(\mathbf{r}-\mathbf{D}) \tag{5}$$

respectively.

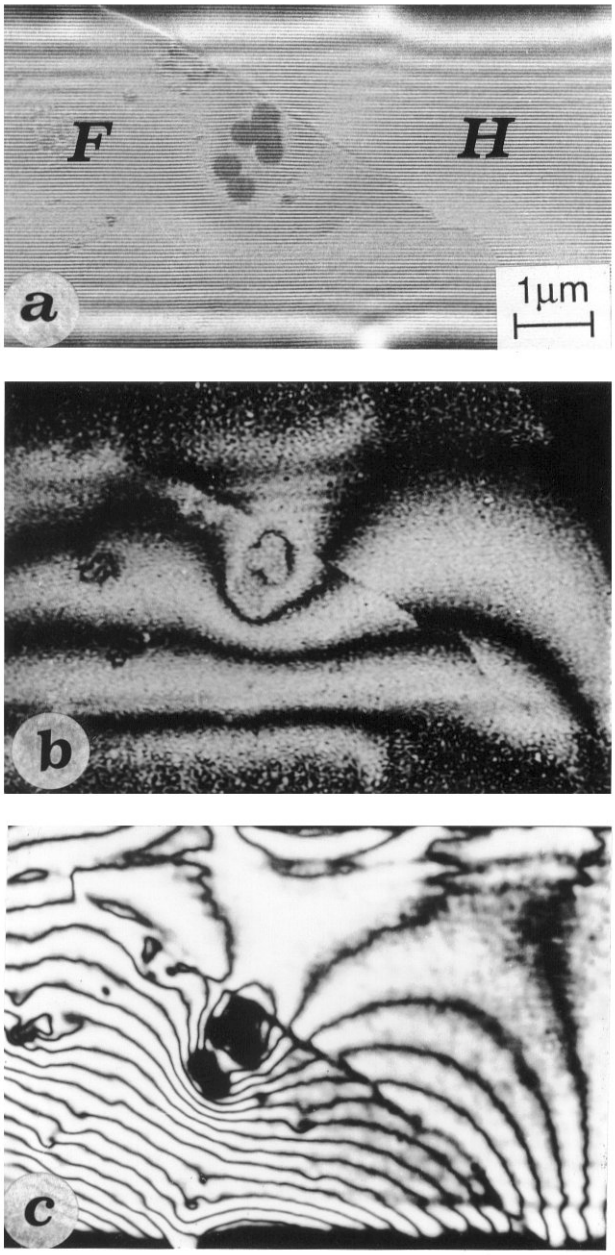

Figure 2. (**a**) Double exposure electron hologram of electrostatic charged spherical particles assembled near a large hole H of a carbon film F. The regions where the interference fringes are blurred map the projected potential distribution. (**b**) Optical reconstruction of the electron hologram of the same region as Figure 2a. (**c**) Four-time phase difference amplified contour map of the same region as Figure 2a.

The apparently innocent correction of the basic equation of holography described by Equation (5) has some far reaching consequences both from the experimental and theoretical points of view. First of all, the fact that the whole phase distribution in the hologram is affected by the field through the perturbed reference wave results in the impossibility of determining unambiguously the carrier spatial frequency and hence the object phase starting from a single hologram. The experimental procedure to extract the most reliable phase difference information (Matteucci *et al.*, 1988, 1991) is recalled in the next section. Yet, it should be borne in mind that, however, careful the hologram processing may be, it will not be possible to avoid the distortion of the recorded object phase which is caused by the perturbation of the reference wave due to long range fields unless experimental conditions are realized for which the interference distance D is much larger than the typical dimension of the field. How large the interference distance should be is a question which can be answered only by computer simulation, as shown in the following.

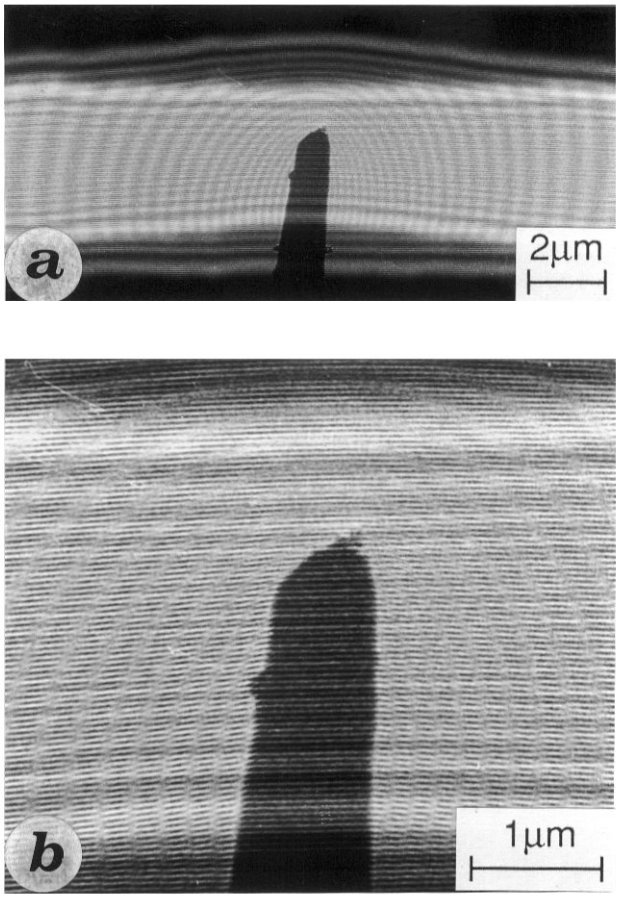

Figure 3. (**a**) Double exposure hologram displaying lines of equal phase difference near the apex of a charged microtip. (**b**) Enlarged view of the near apex region of Figure 3a.

Experimental Results

The considerations outlined in the foregoing section lead to the following procedure for the mapping and amplifying of the phase difference stored in the holograms. When possible, it is worth taking a set of three electron micrographs of the same specimen: (1) a single exposure hologram; (2) an image of the interference field without the object recorded after having withdrawn the specimen from the microscope; this fringe system is used to generate the interferometric wave to extract the phase difference; and (3) a double exposure hologram obtained by recording on the same plate both interferograms (1) and (2); this latter directly furnishes the map of the phase difference between the object and the perturbed reference wave and can be used also as a "guide" hologram when optical phase amplification methods are applied (Matteucci *et al*., 1991).

The experiments reported in this section were carried out with a Philips EM400T transmission electron microscope equipped with a field emission gun. A coherent beam illuminates the specimen placed off-axis so that the reference beam travels within an empty space. Condenser lenses are usually strongly excited, in order to have the highest possible lateral coherence on the specimen plane: this means that often it can be safely assumed that the specimen is illuminated by a plane wave. The objective lens is switched off and the microscope operates in the diffraction mode. The electron biprism is inserted at the selected area plane. In this case, the biprism is negatively biased (15 V), giving a virtual hologram on the specimen plane, which becomes a real one in the image plane. The intermediate lens is used to focus the specimen in the recording plane. The final magnification is in the range of 1000-2500X. Exposure times are of the order of 10 seconds.

Figure 2 shows the results of the foregoing procedure applied to the case of charged latex spheres. Figure 2a shows a double exposure electron hologram of two groups of 4 and 2 charged latex spheres respectively. The spheres, 0.31 μm in diameter, are deposited near a large hole H of a thin carbon film F. The most interesting feature of this micrograph is the contrast variation arising from the overlapping of the two interference fringe systems. The regions of strongly reduced contrast (in the form of moire-like bands) map the in-plane projected potential distribution of the electric field without the need to reconstruct the hologram (Matteucci *et al*., 1988, 1991; Chen *et al*., 1989). Moreover, it can be noted that the phase shift introduced by the carbon film F with respect to the wave passing through the hole H of the foil is responsible of the step of the phase lines when they cross the film rim.

If the double exposure hologram is inserted in an in-line optical bench and is illuminated by a plane laser wave, the carrier fringe system is removed in the reconstructed image (Fig. 2b), thus leaving an optical interferogram which displays the map of the phase difference whose trend is the same as that of the foregoing bands, but with a higher contrast.

Since in the reconstruction and processing of a standard hologram taken with a perturbed reference wave no objective criterion exists for the determination of the correct phase difference map condition, i.e., for recovering the object phase unambiguously, the double-exposure hologram is an essential guide in the optical phase amplification process. Figure 2c shows a four times phase difference amplified map of the same region as Figures 2a and 2b. It is interesting to note that the apparently flat phase regions in Figure 2b are now crossed by optical fringes, indicating that the phase indeed varies, although slowly.

As a further example of the capability of electron holography, we present an experimental result concerning our investigations of the electrostatic field around a charged microtip, prepared by thinning a tungsten wire by standard electrochemical process and mounting it on a special specimen holder equipped with electrical contacts connected to an external voltage supply. The tip could then be biased and rotated in order to be perpendicular to the biprism wire.

Figure 3a shows a double exposure hologram, taken with the tip unbiased (reference hologram) and biased with a voltage of about ten volts. Figure 3b shows an enlarged view of the central region. The contrast bands in the double exposure image demonstrate that the field extends over very large distances and may substantially affect regions very far away; thus unwanted long range electric fields out of the field of view of a standard hologram may in fact influence its phase. Accurate measurements therefore require a check of the absence of electric charges over a region much wider than that displayed in the hologram. Another interesting feature of this image is the strong distortion of the biprism wire edges, due to the electric field, when the tip is biased: in particular, this effect introduces an off-set of the two Fresnel fringe systems of the wire. It follows that the Fresnel phase shift cannot be compensated and becomes an unavoidable artefact of the hologram (Frost *et al*., 1995) which can be remedied only by taking the interference field as large as possible.

Theoretical Simulations

In addition to easier specimen preparation with respect to the case of p-n junctions, the two foregoing case studies have the advantage that also theoretical modelling can be carried out in an analytical form.

The field generated by a single dielectric sphere having the total charge Q which lies on the carbon film can be,

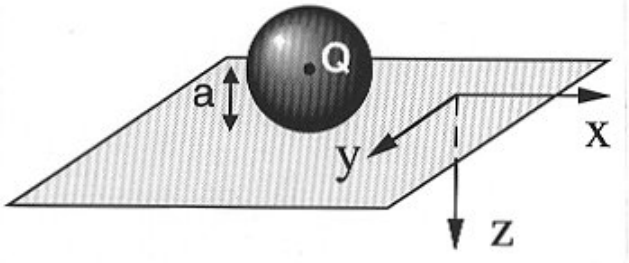

Figure 4. Coordinate system for the potential and phase calculations of a single charged sphere of radius a on a conducting plane, modelled by a point charge Q at its center.

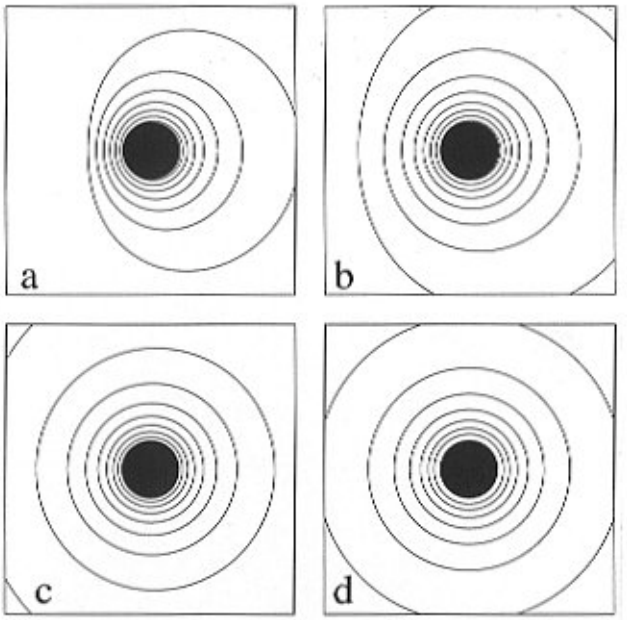

Figure 5. Simulation of the phase difference maps of a charged sphere of radius a on a horizontal conducting plane with increasing interference distance values. (**a**) 5a; (**b**) 10a; (**c**) 20a; and (**d**) infinity.

in fact, satisfactorily modelled by that of an equal point charge located in front of an infinite conducting plane at a distance equal to the radius of the sphere itself, as shown in Figure 4. This is fully justified if one makes the assumption that the charge is isotropically distributed in the body of the sphere and that the distance of the sphere from holes of the supporting carbon film is large compared to the particle size. The thickness of the film can be considered unimportant.

Therefore, for a particle whose center is positioned at the point (x_0, y_0, -a), the potential in the half-space $z < 0$ can be calculated by means of the image charge method (Feynman, 1967) and is given by the expression:

$$V(x,y,z) = (Q/4\pi\varepsilon_0)\,[\{(x-x_0)^2 + (y-y_0)^2 + (z+a)^2\}^{-1/2} - \{(x-x_0)^2 + (y-y_0)^2 + (z-a)^2\}^{-1/2}] \quad (6)$$

while in the half-space $z > 0$, $V(x,y,z) = 0$. The phase shift ϕ can be calculated analytically by inserting Equation (6) into Equation (2). This task is also simply done by Mathematica (Wolfram, 1994) by means of its symbolic computation capabilities, using the built-in object Integrate. The output function can then be used for simulation, as shown in Figure 5 which reports a series of contour plots drawn by the built-in object ContourPlot, with increasing values of the interference distance. The spherical particle is represented by a black disk of radius a and the phase-difference images are plotted over a square of side 10a. Taking a as scale distance, the interference distance is taken respectively as 5a (Fig. 5a), 10a (Fig. 5b), 20a (Fig. 5c) and infinity (Fig. 5d), corresponding to the ideal contour map. It can be ascertained that the main effect of the modulated reference wave is the breaking of the circular symmetry of the equiphase lines. The perturbation diminishes by increasing interference distance, but it is still detectable even for large interference distance *D*.

As the latex particle radius can vary from 0.1 μm up to 3 μm, whereas the interference distance may range from 0.1 μm up to 10 μm depending on the objective lens excitation (on, off or weakly excited), the figures have been plotted without dimensions. To give some numbers, the contour lines in Figure 2 correspond to 2π intervals in a four-time phase amplified image due to the charge of 600 electrons on a spherical latex particle of radius 0.155 μm.

Also, the case of a charged particle on a copper grid, modelled by a vertical conducting plane, can be treated in the same way, as shown by Frost *et al*. (1995); it is only necessary to exchange the *x*-component with the *z*-component in Figure 4. The results corresponding to Figure 5 for these different boundary conditions and for the same values of the square side and interference distances are reported in Figure 6. The vertical conducting plane coincides with the left side of each square (emphasized in bold). In this case, the main effect on the equiphase lines is due to the boundary conditions which somewhat mask the effect of the perturbed reference wave.

In both Figures 5 and 6, the trend of the equiphase lines is very similar to the expected trend of the equipotential lines calculated in the plane of the charge. From these results, it could be inferred that the equiphase lines, actually related to the projected potential distribution, Equation (2), are also a good representation of the equipotential lines.

Owing to the linearity of the basic equations, the foregoing results can be simply generalized to the case of more spheres by adding up the phase shift associated with

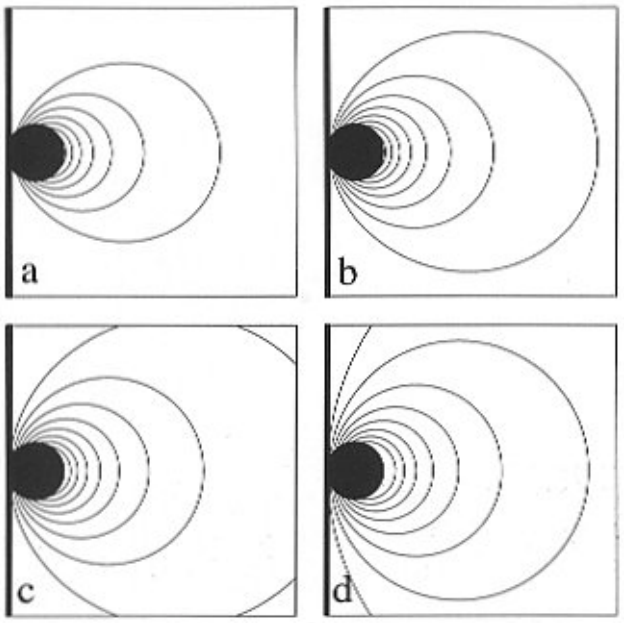

Figure 6. Simulation of the phase difference maps of a charged sphere on a vertical conducting plane with increasing interference distance values. (**a**) 5a; (**b**) 10a; (**c**) 20a; and (**d**) infinity.

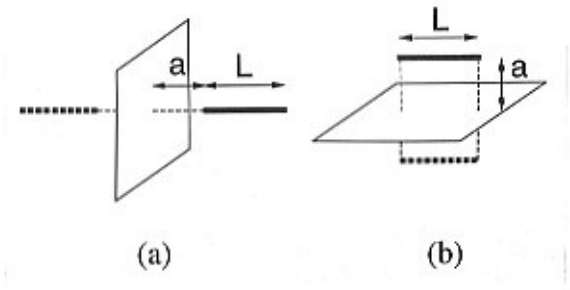

Figure 7. Models for the calculation of the potential of linear charged segment of length L perpendicular (**a**) or parallel (**b**) to a conducting plane. The distance of the apex from the plane is a. The image line charge is dashed.

each single sphere. These simulations confirm satisfactorily the experimental results (Matteucci *et al*., 1991; Frost *et al*., 1995).

The second case study, which emphasizes the importance of a theoretical model for the field is represented by a biased tip. Our theoretical analysis of the electrostatic field around it (Matteucci *et al*., 1992) started by considering (Fig. 7a) two linear charged segments of length L placed in a symmetric position, at a distance a, with respect to a vertical plane. Each segment had a constant and opposite charge density σ. The analytical expression for the potential distribution has been obtained, showing that near and

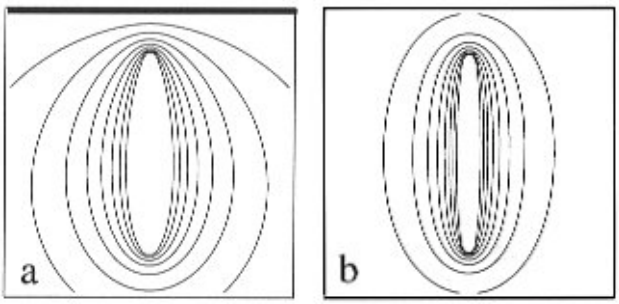

Figure 8. Simulations of the equipotential lines in the plane of a tip (modelled as a linear charged segment) whose axis is (**a**) perpendicular to a plane as sketched in Figure 7a; (**b**) parallel to a plane as sketched in Figure 7b.

around the extremities of the two charged lines, the equipotential surfaces behave approximately as a family of hyperboloids of rotation. Therefore, it was reasonably assumed that this field represented, at least in a first approximation, the field produced by a charged tip in front of a conducting plane, as the shape of the tip closely approximated a hyperboloid. The corresponding phase shift could be obtained analytically after lengthy calculations, which required careful verifications (Matteucci *et al*., 1992).

These same calculations are carried out automatically by Mathematica (Wolfram, 1994), which, starting from the two boundary conditions considered for the charge in front of the plane, by putting $Q = \sigma dt$, allows the analysis of the cases of a line segment in front of or parallel to a conducting plane, provided the integral along t is made perpendicularly, Figure 7a, or parallelly, Figure 7b, to the plane. Therefore, it is possible to investigate, also in this case, the influence of the boundary conditions on the field and the resulting phase shift. Figures 8a and 8b report the trend of the equipotential lines in the plane of the charged line for the two boundary conditions of Figure 7a and 7b respectively. The square is 7a by 7a, the length L of the charged lines has been taken equal to 5a and the vertical plane of Figure 7a, perpendicular to the drawing plane of Figure 8a, coincides with the upper side of the square (emphasized in bold). It can be ascertained that, over distances comparable with a, the distance of the tip from the plane, the boundary conditions affect the potential distribution.

However, when the attention is focused around the tip, over a square of side 0.2a, boundary conditions have much less influence and the obtained results, reported in Figure 9, are almost identical in the two cases.

Figure 9a reports the trend of the equipotential lines in the plane of the tip: they are hyperboloids and the tip is simulated by darkening the surface enclosed by an equipotential line.

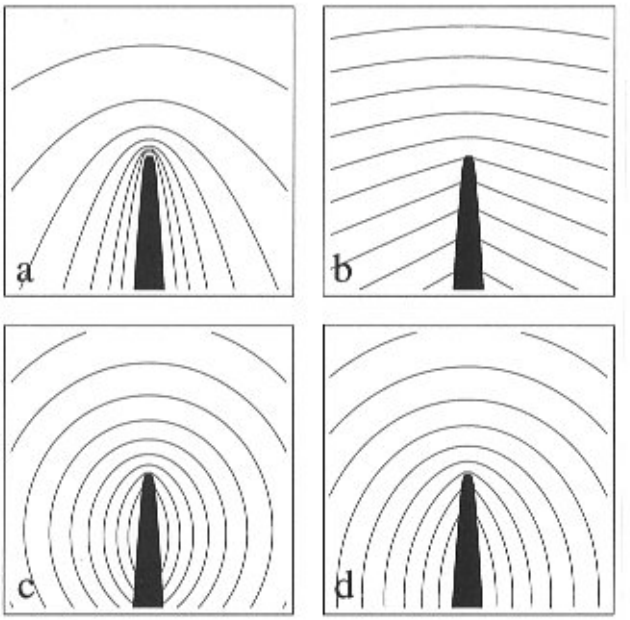

Figure 9. (**a**) Map of the equipotential lines in the tip plane. (**b**) trend of the equiphase lines in the same plane. (**c**) and (**d**) map of the lines of equal phase difference, with interference distances of 0.1a and 0.2a, respectively.

Figure 9b shows the map of the equiphase lines. Their trend is less intuitive than the bidimensional potential distribution because the phase shift, suffered by electrons along their trajectories, is related to the three dimensional potential distribution around the tip integrated along the *z* axis.

Figures 9c and 9d report the trend of the lines of equal phase difference when the influence of a perturbed reference wave is taken into account. The interference distances are 0.1a and 0.2a for Figures 9c and 9d, respectively.

Therefore, the case of the charged tip not only shows that equiphase lines are not, in general, representative of the projected equipotential surfaces, but also that it is very cumbersome, if not impossible, to interpret the experimental results without properly taking into account the effect of the perturbed reference wave.

Conclusions

A short review has been given of the main theoretical and experimental problems encountered in the recording and processing of electron holograms when long range electrostatic fields are present.

From the experimental point of view, the importance has been stressed of having two holograms in register (double exposure) in order to avoid misrepresentation of the field obtained with optical methods and phase amplification techniques.

From the theoretical point of view, we have shown that it is important to start with a good model of the field under investigation in order to calculate, simulate and disentangle the effects of the boundary conditions and of the perturbed reference wave on the phase images. These tasks can be successfully and easily performed using the software package Mathematica with its calculus and graphical capabilities.

In particular, the two case studies investigated show that, contrary to naive assumptions, the phase difference lines in general do not represent directly the potential distribution. Moreover, the effect of the perturbed reference wave must be taken into account, in order not to attribute to the bare field under investigation image features due to its long range tail. While we pointed out the importance of modelling, a recent study (Kou and Chen, 1995) is attempting to cope with this problem in a more general way.

Acknowledgements

This research has been supported by funds from the Ministero della Università e Ricerca Scientifica e Tecnologica and from the Istituto Nazionale per la Fisica della Materia. The skillful technical assistance of Mr. Stefano Patuelli is highly appreciated.

References

Chapman JN (1984) The investigation of magnetic domain structures in thin foils by electron microscopy. J Phys D: Appl Phys **17**: 623-647.

Chen JW, Matteucci G, Migliori A, Missiroli GF, Nichelatti E, Pozzi G, Vanzi M (1989) Mapping of microelectrostatic fields by means of electron holography: Theoretical and experimental results. Phys Rev A **40**: 3136-3146.

Feynman RP (1967) The Feynman Lectures in Physics. Vol. 2. Addison-Wesley, Reading, MA.

Frabboni S, Matteucci G, Pozzi G (1987) Observation of electrostatic fields by electron holography: The case of reverse-biased p-n junctions. Ultramicroscopy **23**: 29-38.

Frost BG, Allard LF, Völkl E, Joy DC (1995) Holography of electrostatic fields. In: Electron Holography. Tonomura A, Allard LF, Pozzi G, Joy DC, Ono YA (eds). North-Holland, Amsterdam. pp 169-179.

Kou L, Chen J (1995) Eliminating the influence of the perturbed reference wave in electron holography. J Mod Optics **42**: 1171-1178.

Matteucci G, Missiroli GF, Pozzi G (1984) Interferometric and holographic techniques in transmission

electron microscopy for the observation of magnetic domain structures. IEEE Trans Magnetics **20**: 1870-1875.

Matteucci G, Missiroli GF, Chen JW, Pozzi G (1988) Mapping of microelectric and magnetic fields with double-exposure electron holography. Appl Phys Lett **52**: 176-178.

Matteucci G, Missiroli GF, Nichelatti E, Migliori A, Vanzi A, Pozzi G (1991) Electron holography of long-range electric and magnetic fields. J Appl Phys **69**: 1835-1842.

Matteucci G, Missiroli GF, Muccini M, Pozzi G (1992) Electron holography in the study of the electrostatic fields: The case of charged microtips. Ultramicroscopy **45**: 77-83.

Matteucci G, Missiroli GF, Pozzi G (1996) Electron holography of electrostatic fields. J. Electron Microsc **45**: 27-35.

Missiroli GF, Pozzi G, Valdrè U (1981) Electron interferometry and interference electron microscopy. J Phys E: Sci Instrum **14**: 649-671.

Möllenstedt G, Düker H (1956) Beobachtungen und Messungen an Biprisma-Interferenzen mit Elektronenwellen (Observations and measurements on biprism-interference with electron waves). Z Phys **145**: 377-397.

Wolfram S (1994) Mathematica: A System for Doing Mathematics by Computer. 2.2. Addison-Wesley, Redwood City, CA.